Available online at www.sciencedirect.com

SciVerse ScienceDirect

Ceramics International 38 (2012) 5757–5767

CERAMICS INTERNATIONAL

www.elsevier.com/locate/ceramint

A comparative study of SiAlON ceramics

Awadesh Kumar Mallik [a,*], Nurcan Calis Acikbas [b], Ferhat Kara [c], Hasan Mandal [d], Debabrata Basu [a]

[a] CSIR-Central Glass & Ceramic Research Institute, 196, Raja S.C. Mullick Road, Kolkata 700032, India
[b] Department of Mechanical and Manufacturing Engineering, Bilecik University, Bilecik, Turkey
[c] Anadolu University, Department of Materials Science and Engineering, Eskisehir, Turkey
[d] Sabanci University, Istanbul, Turkey

Received 20 January 2012; received in revised form 6 April 2012; accepted 6 April 2012
Available online 15 April 2012

Abstract

Two different varieties of Si_3N_4 powders were used to prepare SiAlON ceramics. 100% β-Si_3N_4 was used from refractory grade powders (B1) and another purer 98% α-Si_3N_4 (50A) powder was used to prepare the SiAlON samples. Since SiC + SiAlON composites reportedly perform better, batches were prepared with 15% SiC addition to the refractory powders (B1) and 17.5% SiC was added to the other SiAlON composition (50A). The samples were gas pressure sintered at 1840 °C and at 22 bar with 1 h dwelling time. Thereby, we could achieve 97–98% theoretical density. The hardness was recorded 14–17 GPa while fracture toughness varied from 4.3 to 5 MPa $m^{1/2}$. Fretting experiments showed initial running-in period of 300 cycles for all the tribo-couples. After which, the steady state coefficient of frictions (COF) were achieved. Steel ball of 10 mm diameter, fretting against 50A composition, showed 0.6 average steady state COF while the same composition while fretting against alumina ball of the same diameter, showed 0.57 average steady state COF. Results have been compared with SiAlON composition derived from refractory powder (B1) and found that the 50A composition performs better under identical test conditions. Moreover, cytocompatibility study also suggests that the investigated 50A composition can be used as substrate to support cell adhesion and proliferation of L929 mouse fibroblast cell lines whereas B1 composition derived from refractory powders are toxic in nature.

Keywords: C. Friction; C. Mechanical properties; D. SiAlON; Biocompatibility

1. Introduction:

Silicon nitride (Si_3N_4) ceramics and silicon-aluminium-oxinitride (SiAlON) ceramics are very important class of engineering ceramics. Traditionally alumina has been in use for structural engineering applications but alumina has high hardness and low fracture toughness, whereas silicon nitride ceramics have comparable hardness but very high in situ fracture toughness. Due to higher crack propagation resistance property of nitride ceramics, they are preferred over alumina ceramics in tribological application, specially fretting wear, where a relative cyclic motion between two surfaces, having a non-uniform distribution of local relative displacement at their contact is involved [1,2]. It is reported that silicon nitride ceramics will perform better under fretting wear contact [3–7]. Fretting contact between femoral stem and ceramic femoral ball at the neck region is a potential biotribological application of this class of ceramics. Attempt has been made to use silicon nitride and silicon carbide class of non-oxide ceramics for total hip arthroplasty (THA) applications [8]. This class of materials have been found to be bio-compatible [9–13], but their derivative oxinitrides or SiAlON + SiC composites have not extensively been investigated for biotribological load bearing applications [14–16].

Moreover, the cost of synthesising phase pure silicon nitride ceramics is high due to low diffusion constant. Here comes the development of new class of ceramic alloy, SiAlON ceramics, where Si atoms are replaced by Al and N atoms are replaced by O atoms. SiAlONs have higher chemical resistance, higher oxidation resistance in compare to Si_3N_4. Presence of Al reduces the eutectic temperature by 200 °C, forming grain

* Corresponding author. Tel.: +91 33 24733476/69; fax: +91 33 24730957.
E-mail addresses: amallik@cgcri.res.in, awadesh.mallik@gmail.com (A.K. Mallik).

0272-8842/$36.00
http://dx.doi.org/10.1016/j.ceramint.2012.04.022

boundary glasses more easily and so SiAlONs are easy to sinter. They are having equivalent properties to that of pure silicon nitride ceramics [17–26].

Traditionally alumina ceramics are dominating the structural engineering market (more than 90%); whereas due to high fabrication cost of silicon nitride ceramics, although they perform better than alumina, their application is restricted [27]. But if we can reduce the development cost of nitride/oxinitride class of materials, they have the potential of replacing alumina ceramics in structural engineering applications. The aim of the study was the development of cost effective SiAlON ceramics production technologies to use these materials for biotribological applications. There are many different Si_3N_4 starting powders available in the market. The prices of them vary from 4 to 6 USD/kg for poor quality refractory powders to over 100 Euro/kg for fine and pure quality powders. Starting compositions play an important role in determining the amount of replacement of *m*(Si–N) bonds by *m*(Al–N) bonds and *n*(Si–N) bonds by *n*(Al–O) bonds; and these two variants namely α-SiAlON and β-SiAlON have quite distinct properties.

Microstructural characteristics of SiAlON ceramics are affected by the nature of starting Si_3N_4 powder, sintering additives and obviously by processing conditions. Generally, two forms of silicon nitride exist as starting powder: α-Si_3N_4 and β-Si_3N_4. α-Phase has higher reactivity and is preferred over β-Si_3N_4 as the former has solution re-precipitation tendency into forming elongated β-Si_3N_4 morphology after α → β phase transformation (1410 °C) during sintering [28–30]. Whereas, elongated grain formation and densification are rather difficult, when β-Si_3N_4 powder is used as starting powder [31]. Influence of sintering additive and sintering conditions on microstructural evolution, especially on grain growth have been studied in detail [32,33]. In situ composite microstructures with high fracture toughness can be obtained by gas-pressure sintering of Si_3N_4 ceramics at higher temperatures (>1800 °C) or by heat treating the sintered sample at high temperatures [34–37]. Ekstrom et al. [38] used five different Si_3N_4 powders, containing up to 15% β-Si_3N_4 and Li et al. [39] used three different Si_3N_4 starting powders with similar particle size, but different α:β phase ratios (100α, 50α:50β and 100β). Rosenflanz [40] observed that coarse β-Si_3N_4 powders (*d*50: ~3 μm) delayed transformation to α-SiAlON. Acikbas et al. [41] evaluated the effect of using different starting powder with varying particle sizes on the microstructure and phase development as well as to correlate these with the mechanical properties. The starting β-Si_3N_4 powder (Beijing Chanlian-Dacheng Trade Co., Ltd., China) was produced by combustion synthesis and consisted of 100% β-Si_3N_4 phase. For comparative purpose, an α-Si_3N_4 powder with about 2.1 μm particle size (Grade S, HC-Starck) was also used by them. They observed that marked differences in microstructures can be obtained by starting with different particle sizes of β-Si_3N_4 powders. Initial particle size was of primary importance to achieve bimodal microstructure and hence, improved fracture toughness. A good combination of hardness of around 12 GPa and indentation toughness of 6.4 MPa $m^{1/2}$ could be obtained in ceramics sintered from finest (≤0.5 μm) β-Si_3N_4 powders [7,41,42]. In the present study we continue to work on with the same starting β-Si_3N_4 refractory powders (B1) and have compared this B1 with another SiAlON composition 50A, derived from purer source of UBE powders (α-Si_3N_4). Both the starting Si_3N_4 powders, namely B1 and 50A, were mixed with some SiC addition to enhance their properties. Here, we have tried to compare the fretting wear performance, cell adhesion behaviour and cytotoxicity of these compositions.

2. Materials and methods

2.1. Sample preparation

Two different varieties of Si_3N_4 powders were used to prepare SiAlON ceramics. 100% β-Si_3N_4 (B1) was used from refractory grade powders and another purer source of powder with 98% α-Si_3N_4 (50A) was used to prepare the SiAlON samples. Since SiC + SiAlON composites reportedly perform better [14], batches were prepared with 15% SiC addition to refractory powders (B1) and 17.5% SiC was added to the other SiAlON composition (50A). These powders are having varying amount of impurities. Tables 1 and 2 describe the nomenclatures for starting Si_3N_4 powders. As the as-received refractory powders (B) were having bigger grain sizes, attrition milling was done to reduce the grain sizes of the starting Si_3N_4 powders to about 1 μm level. Table 3 describes the nomenclature after attrition milling. The numbers in the nomenclature indicates average grain sizes.

Phase analysis was done using Cu Kα radiation by Rigaku Rint 2000 X-ray device. Average α–β proportions are obtained from the intensities of (1 0 2) and (2 1 0) planes for α-SiAlON, and for β-SiAlON, proportions are obtained from intensities of (1 0 1) and (2 1 0) according to the formula:

$$\frac{I_\beta}{I_\beta + I_\alpha} = \frac{1}{1 + K\{(1/w_\beta) - 1\}}$$

In this formula I_α and I_β show the intensities of α-SiAlON, and β-SiAlON, w_β is the weight fraction of β-SiAlON, *K* is the constant of [0.518 β (1 0 1) − α (1 0 2) and 0.544 β (210) − α (210)].

Pure SiC powder from Saint Gobin was added in varying amount (15%, 17.5%) to the UBE powders (50A) and to the

Table 1
Powder suppliers specification.

Powder	Code	α:β phase ratio	d50 (μm) as-received	Production method
UBE E10	50A	98α:2β	0.5	Diimide
Refractory powder	B1	100β	4.7	Combustion synthesis

Table 2
Impurities present in the starting Si_3N_4 powder.

	50A	B	B1
% α-Si_3N_4	98	0	0
% β-Si_3N_4	2	100	100
O	<1.4	≤3	≤3
C	<0.2	–	–
Fe	<100 ppm	≤1	≤1
Fe_2Si	–	√	√
Fe_3Si	–	√	√
SiO_2	–	√	√
Si	–	√	√
Ca	<10 ppm	–	–
Al	<50 ppm	–	–
Cl	<100 ppm	–	–

Table 3
Powder specification after attrition milling.

Powder	Code	d50 (μm)
β-Si_3N_4	B2	2
	B1	1
	B0.5	0.5

refractory grade Si_3N_4 powders (B1). Again sintering additives (CeO_2, $CaCO_3$, Y_2O_3, Sm_2O_3, Yb_2O_3) were added to these mixtures. Depending on the cation sizes (which go to the interstitial sites) and temperature, these additives stabilises α-SiAlON phase. In addition to these, required amount of AlN and Al_2O_3 were also added to each composition to get substitutional solid solution of Si_3N_4, i.e. SiAlON phase. Table 4 describes the detail batch calculations of the two batches (B1 and 50A) prepared.

40 g of powder from each batches were weighed and the planetary ball milling was done for preparation of SiAlON composites with SiC (B1 + 15% SiC, 50A + 17.5% SiC). The slurries were dried in a round bottom flask drier evacuated to 150 mbar pressure and were stored in oven. All the powders were passed through the 250 μm sieve mesh size and were kept in plastic pouch for pressing into pellets. From each set of powders, 2 g of powder were poured inside cylindrical mould. The inner bore diameter of the mould was 15 mm. 40 kg/cm^2 pressure was applied to prepare the pellet by hydraulic hand press. Silicone lubricant was used inside the mould before pouring the powder. Afterwards, these pellets were cold isostatically pressed inside latex moulds with 300 MPa pressure and with no holding time. As 2 g of quantity were used to make one pellet, so from each batch of powders 6 pellets were made. Altogether 12 such pellets were made out of two batches of powders.

2.2. Gas pressure sintering

One GPS furnace was used with 22 bar and 2000 °C capacity. The computer programme was set to 22 bar pressure and 1840 °C temperature. 10 °C/min ramping rate was used throughout the heating cycle. An optical pyrometer read the furnace temperature once it reached 1100 °C (red hot condition). During initial heating-up period unto pre-sintering temperature, gas pressure was increased gradually starting from 100 mbar to 5 bar. There was 1 h dwelling time at pre-sintering temperature of 1790 °C at 5 bar pressure. Once 1840 °C sintering temperature is reached gas pressure was increased to 22 bar. After holding for 1 h at 1840 °C the power supply was cut off automatically to the heating elements. The furnace was left to cool down to ambient. The gas pressure was maintained at 17 bar for 3.5 h to help cooling. Afterwards the gas was released to bring the pressure to 1 bar within 20 min.

The 22 bar GPS pellets were characterised for density measurements using Archimedes principle. The samples were kept inside water and put it on a hot plate at 300 °C for 2 h to boil. After 2 h, samples were taken out and suspended weight in water was measured along with the weight after soaking in a tissue paper. The samples were kept inside the oven (50–60 °C) for 40 min to make them dry and again the dry weights of the samples were measured to obtain density.

2.3. Mechanical characterisation

2.3.1. Hardness and fracture toughness

The cross section of mirror polished samples were indented with 10 kg load and for 10 s by Vickers indenter and the average of three measurements were reported as hardness. Fracture toughness was calculated using equation [43]:

$$K_{IC} = \frac{0.15 \times k \times HV \times a^{1/2} \times (c/a)^{-3/2}}{\varphi}$$

where F is the applied load (N), a the average half diagonal length of indentation (mm), c the crack length and k, φ are the constants.

2.3.2. Fretting wear

The fretting experiments had been performed on a computer controlled tribometer (DUCOM model TR281-M) under dry unlubricated ambient conditions (room temperature 23–25 °C; relative humidity measured and maintained at 50–55%). The details of the experimental set up can be found elsewhere [44]. The ball-on-plate configuration was used and fretting vibration at the contact was actuated by a linear relative displacement of

Table 4
Batch calculation[a] of B1 and 50A samples.

Sample name	Si_3N_4	AlN	Al_2O_3	$CaCO_3$	SiC (Saint Gobin)	Y_2O_3	Sm_2O_3	Yb_2O_3
B1 + 15% SiC *or B1*	84.99	4.13	1.156	0.1946	6	2.28	7.346	–
50A + 17.5% SiC *or 50A*	25.07	3.81	2.475	0.4686	7	–	0.541	0.6138

[a] Weights are in g.

constant stroke (mode I, linear displacement sliding). The flat sample was mounted on a translation table, which oscillated at the required displacement with desired frequency by means of a stepping motor. The displacement of the sample was monitored by an inductive displacement transducer, and the friction force was measured with a piezoelectric transducer attached to the holder that supported the counterbody. The friction coefficient was calculated from the on-line measured tangential force. During the test, fretting loops were recorded at a chosen time interval. A fretting loop gave the evolution of the tangential force as a function of the displacement amplitude during each cycle. The friction coefficient (COF) was further evaluated from the average of the two plateau values of the tangential force in the fretting loop, as described elsewhere [45]. In the present investigation, we had chosen a load of 8 N with duration of 45,000 cycles (see Fig. 3). For comparative reasons, all the tests were performed with identical experimental parameters. The only variables were ball counter bodies, namely steel, alumina and SiAlON balls (Table 5 described the properties of counterbodies).

Detailed microstructural characterisation of the as-worn and cleaned surfaces, of flats has been performed with a scanning electron microscope (FESEM, Gemini, Oxford Instruments).

2.4. Cell culture experiments

First, all samples were diamond polished to get the mirror finish and then surface roughness was measured. In this study, L929 Mouse fibroblast cells were used for cell-culture experiments. Before seeding the cells on sample (in pellet form) surfaces, the cells were revived in tissue culture graded culture plate. The cryo-vial was rapidly thawed and cells were cultured in Dulbecco's modified Eagles medium (DMEM, including 300 mg/l L-glutamine, 2 g/l sodium bicarbonate) supplemented with 10% heat-inactivated FBS (Sigma–Aldrich), 1% of antibiotic antifungal cocktail (10,000 IU penicillin 10 mg streptomycin and 25 μg amphotericin B/ml) at 37 °C temperature in a 5% CO_2 humidified atmosphere. The sub-confluent monolayer was trypsinised using 0.5% trypsin and 0.2% EDTA solution (Sigma Aldrich). 5×10^4 L929 cells/well were seeded on gelatin coated control disk and samples.

2.4.1. Cellular adhesion tests

Prior to cell culture, samples were ultrasonically cleaned, sterilised in autoclave (121 °C, 15 lb pressure) and placed under ultraviolet light in a hood for 30 min. Following this, the sterilised samples were soaked in 70% ethanol. Subsequently, 5×10^4 cells/well was seeded on the samples in 24 well culture plates under standard cell culture condition. Now seeded samples were incubated in CO_2 incubator for 48 h at 37 °C, 5% CO_2 and 95% relative humidity. The cell density was measured by Haemocytometer (improved NEUBAUER, DEEPTH 0.1 mm). After 48 h of culture, the material surface was washed with 1 × PBS and then cells were fixed with 2% glutaraldehyde for 20 min. The cells, adhered on the materials surface, were dehydrated using a series of ethanol solutions (30, 50, 70, 95 and 100%) for 10 min twice at each dilution level and then further dried using hexamethyldisilazane (HMDS, Himedia). The dried samples were sputter coated with gold and detailed analyses of cell adhesion behaviour were carried out using SEM.

2.4.2. MTT assay

The modified colorimetric method of Mosmann [46] has been used to confirm the survival and proliferation of mammalian cells in contact with a material. MTT (3(4,5-dimethylthiazol-2-yl)-2,5-diphenyl tetrazolium bromide) is a rapid colorimetric method and is widely adopted for quantification of cytotoxicity and cell proliferation. The cell proliferation and cytocompatibility were investigated on compositions, B1 + 15 wt% SiC (*B1*), 50A + 17.5 wt% SiC (*50A*), and control disk. The samples were seeded at approximate 5×10^4 cells/well. The MTT assay was performed on 3 days, and 5 days. After the incubation, the sample was washed twice with 1 × PBS and reconstitute MTT (5 mg MTT powder was dissolved in 1 ml DMEM) with 10 μl/100 μl of DMEM culture medium was added. Subsequently, the culture plate was incubated for 4–6 h in CO_2 incubator at 37 °C. In the meantime, culture plate was viewed in the phase contrast microscope (Nikon-Eclipse 80i, Japan) to check the formation of purple formazan crystal. Subsequently, the medium and MTT solution was aspirated and samples were washed with 1 × PBS. The insoluble formazan crystal was dissolved by adding 200 μl of Dimethylsulphoxside (DMSO) and culture plate was rocked to dissolve the formazone crystals. The samples were removed from wells and optical density of the solutions were measured at 540 nm using ELISA Automated Microplate Reader (Bio-Tek, model ELx800). The quantification of the cell proliferation/viability in terms of metabolically active cells was calculated using the formula, % viability = (mean absorbance of sample/mean absorbance of control) × 100.

3. Results and discussion

3.1. Physical characterisation

Fig. 1a shows the X-ray diffraction pattern of the as-received UBE powders (used for composition 50A) whereas Fig. 1b is the XRD micrograph for the refractory powders (B). The X-ray

Table 5
Ball counter-body properties from suppliers' database.

Ball material	HV_5 (GPa)	K_{IC} (MPa $m^{1/2}$)	Roughness (μm)	Elastic modulus (GPa)
Steel (DIN100Cr6, construction grade)	20	7.8	0.02	210
Alumina (99.7% pyre, grade 10)	19	4.0	0.02	300
Si6-zAlzOzN8-z, z=0.3, grade TCQ	15.5	4.7	0.02	310

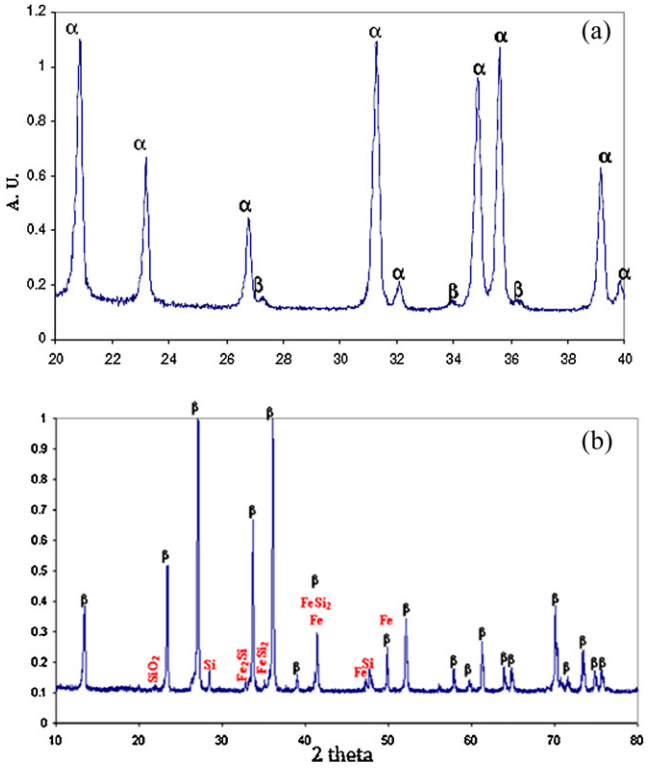

Fig. 1. XRD micrographs of (a) UBE as-received powder, (b) Chinese refractory powder.

micrographs clearly show the phase purity of 50A powders, containing mostly (98%) α-Si_3N_4. On the other hand, X-ray of the refractory grade β-silicon nitride powder shows presence of many impurities with 100% β-Si_3N_4 phase. The impurities have been identified as, SiO_2, Si, Fe, Fe_2Si, $FeSi_2$, etc. Fig. 2 is the scanning electron micrographs of the same 50A powders and B1 refractory powders respectively. Fig. 2a and b are showing sub-micron grains of equiaxed α-Si_3N_4 powder at two different magnifications. Whereas, Fig. 2c and d are showing elongated β-Si_3N_4 powder at 5000× and 10,000× magnifications. The as-received refractory powders were having bigger grain sizes. So attrition milling was done to reduce the grain sizes of the starting β-Si_3N_4 powders to about one micron level (Tables 2 and 3).

Both the Si_3N_4 starting powders were mixed with sintering additives, AlN, Al_2O_3 and SiC powders following definitive procedures as described in Section 2. Then the sample was gas pressure sintered to obtain SiAlON ceramics with desired α–β phase ratios. But unfortunately due to the presence of different impurities (as shown in Table 2) in the starting powders, we never end up with desired phase percentages after sintering. The batch calculation for 50A composition was done so as to get a 50:50 α–β phase ratio and thus have been coded as 50A. On the other hand a phase ratio of 30α:70β was obtained from batch calculation of refractory grade powder. Bulk density of 3.16 for 50A + 17.5% SiC and 3.29 for B1 + 15% SiC were recorded. These values indicate that we have achieved 97.19% and 98.44% of theoretical density for 50A and B1 compositions respectively. The slight decrease in theoretical density for 50A composition is due to addition of 17.5% SiC in compare to 15% SiC for B1 composition. Souza et al. [14] have reported that as we increase the SiC percentages in SiAlON ceramics, we get more porosity in the structure. The explanation is as follows: SiC addition inhibits the rearrangement, and subsequently solution-reprecipitation process of the main phase grains (SiAlON) in the presence of the liquid phase [47–49].

3.2. Mechanical properties

3.2.1. Hardness and fracture toughness

Hardness is found to be much higher for 50A composition, 17.2 GPa, whereas B1 composition gives 14.1 GPa hardness. On the other hand fracture toughness of the 50A composition is much lower than B1 composition (Table 6). This is due to the fact of the presence of elongated β-SiAlON grains in the final microstructure of B1 composition. A well known fact of the SiAlON ceramics is that, equiaxed α-SiAlON grains are responsible for high hardness and elongated β-SiAlON grains provides high fracture toughness. As the B1 composition has more β-SiAlON in comparison to 50A composition, it is giving higher fracture toughness of 5.0 MPa $m^{1/2}$, in compare to 4.3 MPa $m^{1/2}$ of 50A composition. But this increase in fracture toughness for B1 composition comes with loss in hardness values due to decrease in number of α-SiAlON grains. Souza et al. [14] have reported a decrease in hardness and fracture toughness values with increase in percentages of SiC in SiAlON composition. They have plotted 15 GPa hardness and 4.5 MPa $m^{1/2}$ of fracture toughness for SiAlON composition having 15% SiC. Their reported values are well in agreement with our present work.

3.2.2. Fretting wear

SiAlON flats were made to fret against different ball counterbodies. The fretting contact between femoral stem and femoral ball at the neck region of THA is commonly between steel vs. ceramics. So a 50A flat was fretted against steel ball counterbody simulating fretting wear condition of THA. Reason behind choosing alumina ball counterbody was to have harder material fretting against SiAlON ceramics. Again, SiAlON counterbody balls were chosen to study tribological properties of self-mated systems.

For all the above tribocouples, with 10 mm diameter ball counterbodies, Hertzian Contact Pressure (Po) is calculated using the equation:

$$P_o = \left(\frac{3}{2}\right)P_m = \frac{6WE^{*2}}{\pi^3 R^2}$$

The initial contact diameter is given by, $a = (3WR/4E^*)^{1/3}$; where W is the applied load, E^* is effective Elastic modulus, and R is the radius of the ball.

Hertzian contact pressure (P_o) was calculated to be 800 ± 10 MPa, when the initial contact diameter was 60 μm.

Fretting experiments showed initial running-in period of 300 cycles for all the tribo-couples. After which steady state

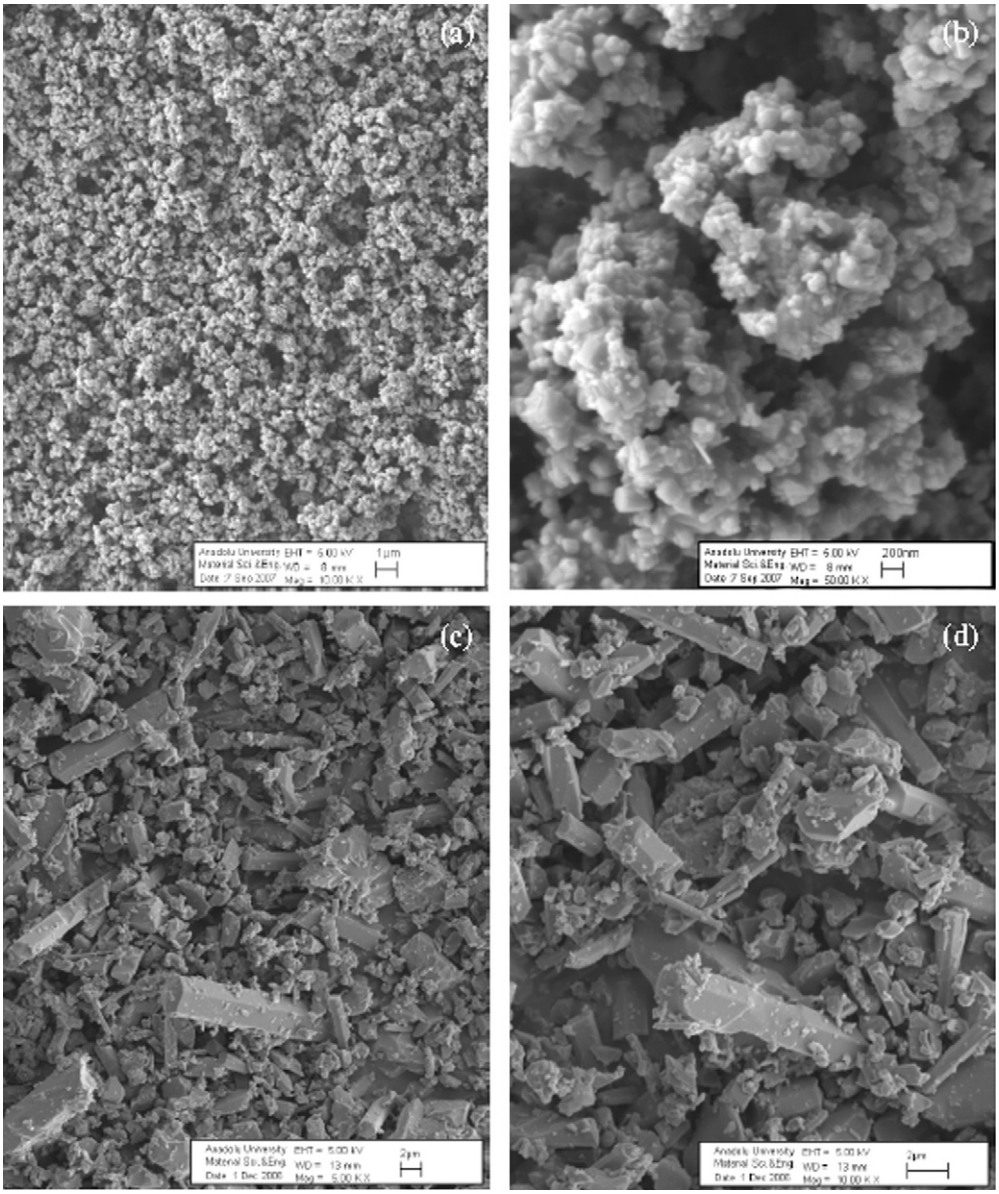

Fig. 2. SEM images of as-received powders, (a) UBE powder at 10,000× magnification, (b) UBE powder at 50,000× magnification, (c) Chinese refractory powders at 5000× magnification, (d) Chinese refractory powders at 10,000× magnification.

coefficient of frictions were achieved. For steel ball of 10 mm diameter fretting against 50A composition shows 0.6 average steady state COF while the same 50A composition while fretting against alumina ball of same 10 mm diameter shows 0.57 average steady state COF. These values are in agreement with the literature [4,6]. Now we wanted to compare the fretting wear behaviour of 50A SiAlON with B1 compositions (made from cheaper refractory grade starting powders). A COF value of 0.66 was achieved when B1 flats were fretted against alumina counterbodies of 10 mm diameter, which is higher than 50A composition. To confirm the better performance of 50A composition, we again repeated the fretting experiments for B1 composition under self-mating conditions, i.e. B1 composition flat was fretted against SiAlON counterbodies with 10 mm diameter. The average steady state COF value achieved was 0.62, which is almost similar to COF values for 50A-vs.-steel, but still higher. So we can conclude that fretting experiments showed SiAlON ceramics with 50A composition give better COF values compare to cheaply available refractory grade B1 composition under fretting contact. The frictional curves are shown in Fig. 4.

Fig. 5 shows the fretting wear scar mark analysis of B1 composition after fretting against alumina ball. Double arrow indicates fretting wear direction. Wear grooves are seen and it is found that the diameter of wear scar is more along the fretting direction than to its orthogonal direction. This difference in wear scar length along the two perpendicular directions is responsible for non-circular (rather elliptical) fretting wear scar mark on the sample. So it is important to look at the wear

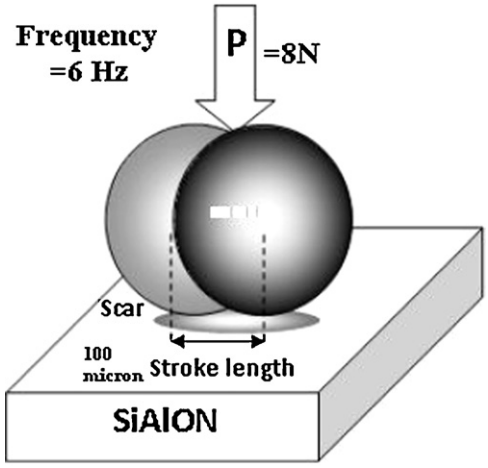

Fig. 3. Schematic of Fretting Test conditions: 10 mm diameter counterbodies, Constants-Stroke length 100 μm, Oscillation frequency 6 Hz, number of cycles (45,000) and normal load (8 N).

Table 6
Physical properties of SiAlON samples (1790 °C is the presintering temperature and sintering was done at 1840 °C, 22 bar pressure and 1 h at each stage was the dwelling time).

Sample	50A	B1
Bulk density	3.16	3.29
Open porosity	0.42	0.63
Percentage theoretical density	97.2	98.5
HV_{10} 10 s GPa	17.2 ± 0.12	14.1 ± 0.11
K_{IC} MPa $m^{1/2}$	4.3 ± 0.09	5.0 ± 0.05

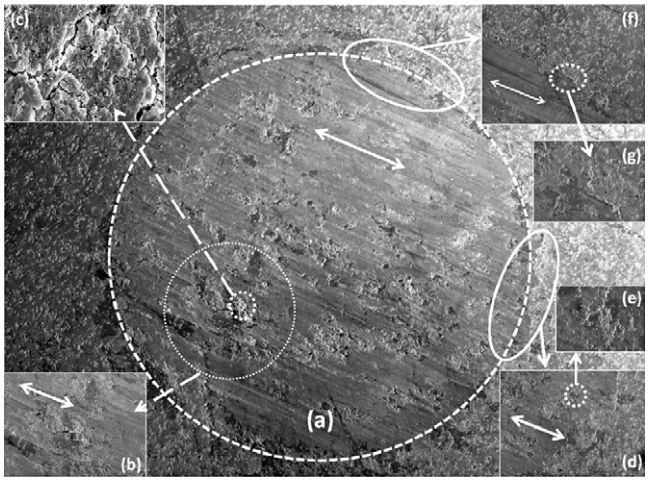

Fig. 5. SEM images revealing the overview and detailed topographical features of B1 + 15% SiC composition after 45 K cycles with fretting conditions: 8 N load, 6 Hz frequency, 100 μm stroke length; Hertzian contact pressure of $P_o \approx 800$ MPa, counterbody: 10 mm diameter alumina ball. (a) Overall view of wear track, double arrow indicates fretting direction, patches of wear debris can be seen, (b) magnified view of the region showing wear debris forming tribolayer, (c) magnified view of tribolayer showing wear particles and cracking of the tribolayer, (d) revealing the topographical features of (a) at the interface between wear scar and flat surface, double arrow indicates the fretting direction, the interface area is the region in the direction of the fretting wear, (e) a magnified view of the dotted area in (d), shows formation of wear debris layer structure, (f) revealing the topographical features of (a) at the interface between wear scar and flat surface, double arrow indicates the fretting direction, the interface area is the region perpendicular to the direction of the fretting, (g) a magnified view of the dotted area in (f) shows formation of wear debris layer structure.

pattern at these two orthogonal directions for better understanding of fretting. Fig. 5b, the magnified view of the circled region of Fig. 5a, shows abrasive wear grooves of 10–20 μm width. Abrasive wear particles under the action of heat and stress form silica rich tribolayers [42]. Cracks are originated and are propagated through these layers, leading to fragmentation of such tribolayers. Crack formation and fragmentation of such tribolayer is evident in Fig. 5c (magnified view of the central position of Fig. 5b).

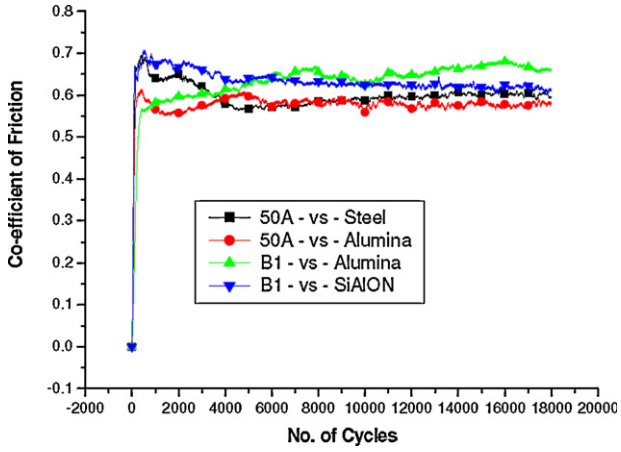

Fig. 4. Friction curves for different tribo-couples under fretting contact.

In order to find out the difference in microstructural features at the ends of two orthogonal directions (along the fretting stroke direction and along the direction perpendicular to the fretting stroke), SEM images (Fig. 5d and f) were taken at the edges of the fretting scar mark. Fig. 5d shows the microstructural features at the fretting-end interface area (region between fretting and non-fretting) in the direction of the fretting (right side of the wear scar, Fig. 5a) and Fig. 5f shows the features present at the interface area perpendicular to the fretting direction (top side of wear scar, Fig. 5a). Fig. 5e (magnified view of the circled region of Fig. 5d) shows formation of wear debris which under the action of heat and stress form tribolayers. These tribolayers are also present in the top side but negligible in amount, Fig. 5g (magnified view of the circled region of Fig. 5f). Hence, top side of the wear scar is cleaner than the interface region on the right side of the wear scar. The reason is, wear debris generated under ploughing action of oscillating counterbody will accumulate at the end of sliding direction; on the contrary very little accumulation of wear debris on the top side region, direction orthogonal to sliding (ploughing action). So the side-end regions of the fretting wear scar (Fig. 5d) are being dirtier than the top-end regions (Fig. 5f).

Fig. 6 shows the fretting wear scar mark analysis of B1 composition after fretting against SiAlON ball. This was done to find out the effect of self-mating condition on fretting

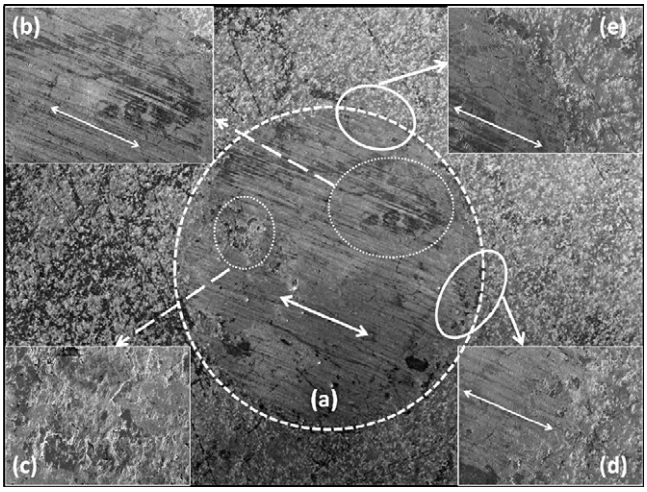

Fig. 6. SEM images revealing the overview and detailed topographical features of B1 + 15% SiC composition after 45 K cycles with fretting conditions: 8 N load, 6 Hz frequency, 100 μm stroke length; Hertzian contact pressure of $P_o \approx 800$ MPa, counterbody: 10 mm diameter SiAlON ball. (a) Double arrow marks indicate the fretting direction; overall view of wear track with big dotted circle, showing wear grooves and wear patches with little or no wear debris, (b) magnified view of the wear patch shows no tribolayer formation, (c) wear patch mark without significant layer structure, (d) SEM images revealing the topographical features of (a) at the interface between wear scar and flat surface, double arrow indicates the fretting direction, the clean interface area is the region along the direction of the fretting (right side of (a)), (e) the clean interface area is the region perpendicular to the direction of the fretting (top side of (a)).

behaviour. Self-mating contact is expected to cause less dirt of wear due to equivalent hardnesses of the ball and the flat. Double arrow indicates fretting wear direction. Wear grooves are seen and it is found that diameters of wear scar are almost equal along the fretting direction and to the direction perpendicular to fretting. In order to find out the difference in microstructural features among these two directions (as we did it for Fig. 5a), perpendicular to each other, SEM images (Fig. 6d and e) were taken at the edges of the scar mark. Fig. 6d shows the microstructural features at the interface area along the direction of the fretting (right side of the wear scar, Fig. 6a) and Fig. 6e shows the features present at the interface area perpendicular to the fretting direction (top side of wear scar, Fig. 6a). It is clear from both Fig. 6d and e, that, there is very little formation of abrasive wear particle, as both the regions are clean. The absence of abrasive wear particle can be attributed to the self-mating condition, i.e. as the flat and ball both are made of SiAlON ceramics of comparable hardness (14.1 GPa and 15.5 GPa respectively), little or no abrasive wear took place. On the other hand when softer SiAlON flats (14 GPa) were fretted against hard alumina ceramic ball (19 GPa), abrasive wear took place, which was evident from dirty as-worn surfaces (Fig. 5). Fig. 6b shows the magnified dotted region of Fig. 6a. Wear grooves are found with very small width of 5 μm or so. Black patches are present all over this region. When we magnified another dotted circle of Fig. 6a, we could find similar black patches in Fig. 6c. Now from Fig. 6c it is very clear that the black patches are not at all tribolayers, which are characteristics of such fretting wear [42]. The complete absence of silica rich tribolayers may be attributed to the absence of abrasive wear under self-mating condition. Abrasive wear produces oxygen rich hard wear particles, which form tribolayer under combined action of heat and stress. As SiAlON flat was fretted against SiAlON ball, no abrasive particle generated and thereby no tribolayer formed.

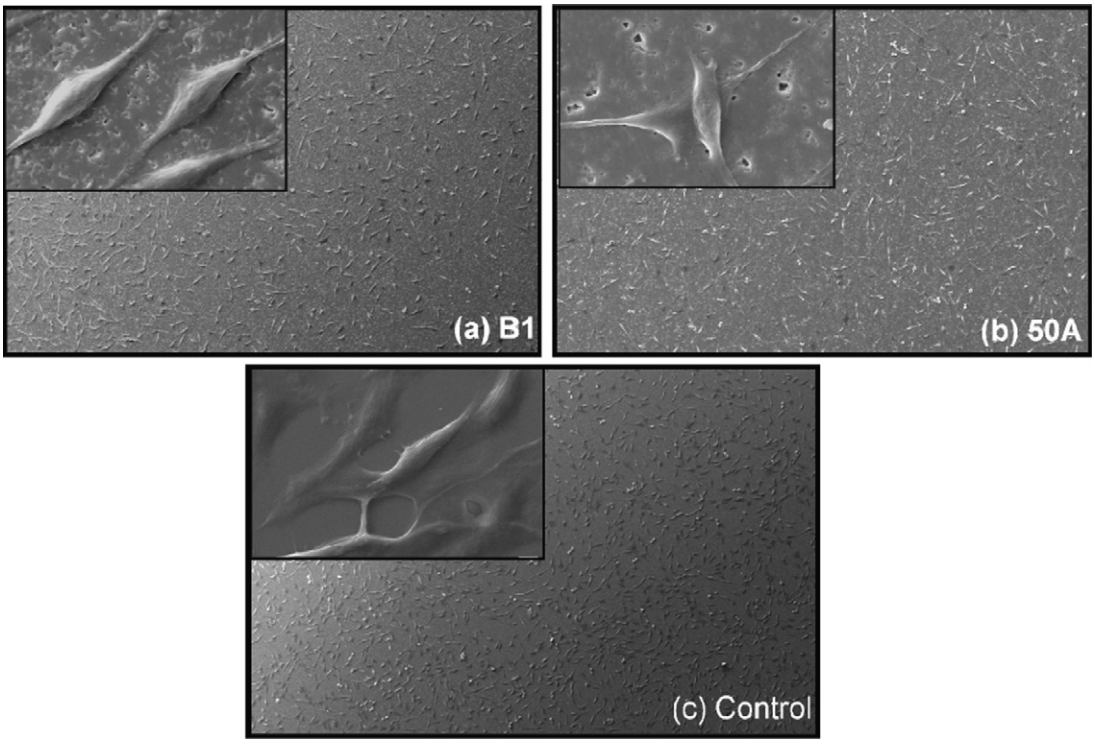

Fig. 7. Low magnification SEM images of L929 fibroblast cell cultured for 48 h on (a) B1, (b) 50A, (c) control with high magnification images at the inset.

3.3. In vitro results

3.3.1. Cellular adhesion behaviour

In order to investigate cell adhesion behaviour of SiAlON compositions, L929 mouse fibroblast cells were used. The reasons for using this particular cell line are that L929 cells can easily proliferate and adhere on most of the biomaterials surfaces, secondly, L929 cells are the typical cell type, which participate in the early stage of wound healing process and moreover, L929 cell line is widely used for preliminary biocompatibility evaluation for a wide range of biomaterials. Fig. 7 shows the scanning electron microscopic evidences of the cellular adhesion of L929 on control, B1, and 50A after 48 h. The images were taken in 200× magnifications to reveal uniform cell growth features over control and sintered samples whereas higher magnification images at the inset of each micrograph were taken at 5000× magnifications to analyse the cell proliferation features. It can be noted that L929 cells are used in compliance with the biocompatibility testing, as outlined in ISO 10993-5 guideline for in vitro test. Therefore, the optimised culture time was 48 h [50]. From low magnification images, it is clear that L929 mouse fibroblast does not show much difference in morphology and adhesion behaviour on samples. Figures in inset clearly reveal the cell proliferation (a coordinated process of growth and division) and cell–cell contacts on both the samples. It has been observed that cell proliferation and cell-to-cell contacts are similar in sintered samples in comparison to control. Cells were fully spread on both the samples with multiple lamellae extended in all the directions (Fig. 7a and b). Other noticeable feature was that L929 showed significantly higher lamellipodium extension.

3.3.2. Cellular viability

It is well known that MTT reagent directly reacts with the mitochondria (Mitochondrial dehydrogenase enzyme) of metabolically active cells. Therefore, the reaction of MTT will be more if more number of metabolically active cells are present. Hence, MTT is widely regarded as one of the quantitative assays to determine the cytotoxicity of the materials, detecting the cell viability/proliferation on the sample surface. The measured optical density, as recorded with ELISA plate reader is directly proportional to the number of viable cells in the culture medium. Fig. 8 plots the quantified data on cell proliferation using MTT assay for 3 days and 5 days after cell proliferation. The results show that cell proliferation on SiAlON samples is comparable with control disc after 3 days. The results are presented as %viability of cells with reference to control disc. For both the samples, the numbers of metabolically active cells are statistically lower than that of the control (see Fig. 8). No significant difference in the cell viability between control and SiAlON samples had been noticed after 3 days of experiment. Only B1 showed less cell viability as compare to 50A sample. After 5 days, the MTT results showed high cell toxicity on sample B1 which were made from refractory grade powders. It was evident from Fig. 1b that the refractory powder B1 contained Si, Fe, SiO_2, Fe_2Si, $FeSi_2$, etc. impurities (Table 2) which were detrimental for cell survival, whereas a pure source of precursor powders (UBE), used for making 50A composition, did not contain any such impurities other than Fe, Al, Ca, Cl at ppm level. These impurities were present at minimal level in 50A and may be the reason behind 50A supporting cell proliferation even after 5 days. Thus, 50A is biocompatible, whereas B1 is not.

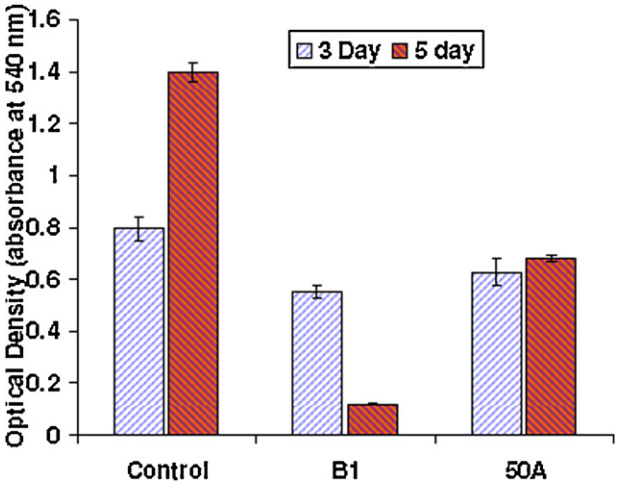

Fig. 8. Viabilities of L929 cells were determined by measuring the optical density (absorbance at 540 nm) in MTT assay of control, B1 and 50A SiAlON samples after 3 days and 5 days. Error bars represent the standard deviation of mean.

4. Conclusions

Two Si_3N_4 starting powders with different purity levels and α, β amounts were used to fabricate SiAlON ceramics. SiC was added to improve their tribological performance and found not to affect their biological responses. If we compare these two SiAlON ceramics (B1 and 50A), following conclusions can be drawn:

- Lower COF of 0.57 was achieved with 50A composition which is about 16% better compare to fretting friction for B1 sample under identical conditions.
- 17.2 GPa hardness of 50A sample with 4.3 MPa $m^{1/2}$ fracture toughness which is 22% higher than hardness of B1 sample and 16% less than fracture toughness of B1 sample.
- Refractory grade B1 composition performed better only under self mating fretting contact.
- 50A composition supports cell adhesion and is non-toxic; whereas B1 composition is cytotoxic.

Acknowledgements

This work was financially supported by CSIR-India and TUBITAK-Turkey under international S&T collaborative program titled ‘‘Development of SiAlON ceramics for tribological applications’. Merve Yaygingol assisted in preparing the SiAlON samples. Alok Kumar helped in carrying out fretting wear and cell culture experiments. Authors thank Prof. Bikramjit Basu for allowing us to access his laboratory facilities.

References

[1] R.B. Waterhouse, Fretting Wear, ASM Handbook: Friction, Lubrication and Wear Technology, ASM, Materials Park, OH, 1992.

[2] M. Varenberg, I. Etsion, G. Halperin, Slip index: a new unified approach to fretting, Tribology Letter 17 (2004) 569–573.

[3] B. Basu, Manisha, N.K. Mukhopadhyay, Understanding the mechanical properties of hot pressed Ba-doped S-phase SiAlON ceramics, Journal of the European Ceramic Society 29 (2009) 801–811.

[4] Manisha, B. Basu, Tribological properties of a hot-pressed Ba-doped S-phase SiAlON ceramic, Journal of the American Ceramics Society 90 (6) (2007) 1858–1865.

[5] B. Basu, M. Lewis, M.E. Smith, M. Bunyard, T. Kemp, Microstructure development and properties of novel Ba-doped phase SiAlON ceramics, Journal of the European Ceramic Society 26 (2006) 3919–3924.

[6] B. Basu, J. Vleugels, M. Kalin, O. Van Der Biest, Friction and wear behaviour of SiAlON ceramics under fretting contacts, Materials Science and Engineering A 359 (2003) 228–236.

[7] A.K. Mallik, K. Madhav Reddy, N.C. Acikbas, F. Kara, H. Mandal, D. Basu, B. Basu, Influence of SiC addition on tribological properties of SiAlON, Ceramics International 37 (7) (2011) 2495–2504.

[8] M.N. Rahaman, A. Yao, B.S. Bal, J.P. Garino, M.D. Ries, Ceramics for prosthetic hip and knee joint replacement, Journal of the American Ceramics Society 90 (7) (2007) 1965–1988.

[9] C.R. Howlett, E. McCartney, W. Ching, The effect of silicon nitride ceramic on rabbit skeletal cells and tissue. An in vitro and in vivo investigation, Clinical Orthopaedics and Related Research 244 (1989) 293–304.

[10] R. Kue, A. Sohrabi, D. Nagle, C. Frondoza, D. Hungerford, Enhanced proliferation and osteocalcin production by human osteoblast-like MG63 cells on silicon nitride ceramic discs, Biomaterials 20 (13) (1999) 1195–1201.

[11] A. Sohrabi, C. Holland, R. Kue, D. Nagle, D.S. Hungerford, C.G. Frondoza, Proinflammatory cytokine expression of IL-1beta and TNF-alpha by human osteoblast-like MG-63 cells upon exposure to silicon nitride in vitro, Journal of Biomedical Materials Research 50 (1) (2000) 43–49.

[12] C.C. Sorrell, R.K. Druitt, C.R. Howlett, E. McCartney, Results of 15-year clinical study of reaction bonded silicon nitride intervertebral spacers, in: World Biomaterials Congress, Sydney Australia, 2004.

[13] A. Yamamoto, R. Honma, M. Sumita, T. Hanawa, Cytotoxicity evaluation of ceramic particles of different sizes and shapes, Journal of Biomedical Materials Research: Part A 68 (2) (2004) 244–256.

[14] J.V.C. Souza, C. Santos, C.A. Kelly, O.M.M. Silva, Development of α-SiAlON–SiC ceramic composites by liquid phase sintering, International Journal of Refractory Metals & Hard Materials 25 (2007) 77–81.

[15] C. Santos, S. Ribeiro, J.K.M.F. Daguano, S.O. Rogero, K. Strecker, C.R.M. Silva, Development and cytotoxicity evaluation of SiAlONs ceramics, Materials Science and Engineering C 27 (2007) 148–153.

[16] A. Kumar, A.K. Mallik, N.C. Acikbas, M. Yaygmgol, F. Kara, H. Mandal, D. Basu, K. Biswas, B. Basu, Cytocompatibility property evaluation of gas pressure sintered SiAlON–SiC composites with L929 fibroblast cells and Saos-2 osteoblast-like cells, Materials Science and Engineering C 32 (3) (2012) 464–469.

[17] A. Rosenflanz, I.W. Chen, Kinetics of phase transformations in SiAlON ceramics. I: effects of cation size, composition and temperature, Journal of the European Ceramic Society 19 (1999) 2325–2335.

[18] A. Rosenflanz, I.W. Chen, Kinetics of phase transformations in SiAlON ceramics. II: reaction paths, Journal of the European Ceramic Society 19 (1999) 2337–2348.

[19] H. Mandal, New developments in α-SiAlON ceramics – sialons and related nitrogen ceramics, Journal of the European Ceramic Society 19 (1999) 2349–2357.

[20] G.Z. Cao, R. Metselaar, α-SiAlON ceramics: a review, Chemistry of Materials 3 (2) (1991) 242–252.

[21] V.A. Izhevskiy, L.A. Genova, J.C. Bressiani, F. Aldinger, Progress in SiAlON ceramics, Journal of the European Ceramic Society 20 (2000) 2275–2295.

[22] F.L. Riley, Silicon nitride and related materials, Journal of the American Ceramic Society 83 (2) (2000) 245–265.

[23] P.F. Becher, E.Y. Sun, K.P. Plunket, K.B. Alexander, C.H. Hsueh, H.T. Lin, S.B. Waters, C.G. Westmoreland, E.S. Kang, K. Hirao, M.E. Brito, Microstructural design of silicon nitride with improved fracture toughness. I: effects of grain shape and size, Journal of the American Ceramic Society 81 (11) (1998) 2821–2830.

[24] E.Y. Sun, P.F. Becher, K.P. Plunket, C.H. Hsueh, K.B. Alexander, S.B. Waters, K. Hirao, M.E. Brito, Microstructural design of silicon nitride with improved fracture toughness. II: effects of yttria and alumina additives, Journal of the American Ceramic Society 81 (11) (1998) 2831–2840.

[25] R.K.A. Lakshminrayanan, A.A. Hoffman, Ultra-low wear ceramic composite bearings, in: Proceedings in Bioceramics, Palm Springs, CA, 2001.

[26] M. Amaral, M.A. Lopes, R.F. Silva, J.D. Santos, Densification route and mechanical properties of Si_3N_4-bioglass biocomposites, Biomaterials 23 (2002) 857–862.

[27] Editorial: Engineering ceramics market outlook, American Ceramic Society Bulletin 82 (11) (2003) 16–17.

[28] S. Wild, P. Grieveson, K.H. Jack, Special ceramics, in: P. Popper (Ed.), Stoke-on-Trent, vol. 5, British Ceramic Research Association, 1972, p. 385.

[29] D.D. Lee, S.J.L. Kang, G. Petzow, D.K. Koon, Effect of α to β phase transition on the sintering of silicon nitride ceramics, Journal of the American Ceramic Society 73 (1990) 767–769.

[30] H. Mandal, D.P. Thompson, T. Ekstrom, Reversible α-sialon transformation in heat-treated SiAlON ceramics, Journal of the European Ceramic Society 12 (1993) 421–429.

[31] S.K. Lee, K.S. Lee, B.R. Lawn, D.K. Kim, Effect of starting powder on damage resistance of silicon nitrides, Journal of the American Ceramic Society 81 (1998) 2061–2070.

[32] S. Hampshire, K.H. Jack, in: F.L. Riley (Ed.), Progress in Nitrogen Ceramics, Martinus Nijhoff Publishers, Boston, 1983, pp. 225–230.

[33] G. Ziegler, J. Heinrich, G. Wotting, Relationships between processing, microstructure and properties of dense and reaction-bonded silicon nitride, Journal of Materials Science 22 (1987) 3041–3086.

[34] M. Mitomo, H. Tsutsumi, S. Tanaka, S. Uenosono, F. Saito, Grain growth during gas-pressure sintering of β-silicon nitride, Journal of the American Ceramic Society 73 (1990) 2441–2445.

[35] M. Mitomo, H. Hirotsuru, H. Suematsu, T. Nishimura, Fine-grained silicon nitride ceramics prepared from β-powder, Journal of the American Ceramic Society 78 (1995) 211–214.

[36] C.J. Lee, J.I. Chae, D.J. Kim, Effect of β-Si_3N_4 starting powder size on elongated grain growth in β-Si_3N_4 ceramics, Journal of the European Ceramic Society 20 (2000) 2667–2671.

[37] N. Hirosaki, Y. Akimune, M. Mitomo, Effect of grain growth of β-silicon nitride on strength, Weibull modulus, and fracture toughness, Journal of the American Ceramic Society 76 (1993) 892–894.

[38] T. Ekstrom, N. Ingelstrom, R. Brage, M. Hatcher, T. Johansson, α–β SiAlON ceramics made from different silicon nitride powders, Journal of the American Ceramic Society 71 (1988) 1164–1170.

[39] Y.W. Li, P.L. Wang, W.W. Chen, Y.B. Cheng, D.S. Yan, Phase formation and microstructural evolution of Ca α-sialon using different Si_3N_4 starting powders, Journal of the European Ceramic Society 20 (2000) 1803–1808.

[40] A. Rosenflanz, α-SiAlON: phase stability, phase transformations, and microstructural evolutions, PhD thesis, Michigan University, 1997, pp. 178–179.

[41] N.C. Acikbas, R. Kumar, F. Kara, H. Mandal, B. Basu, Influence of β-Si_3N_4 particle size and heat treatment on microstructural evolution of α:β-SiAlON ceramics, Journal of the European Ceramic Society 31 (2011) 629–635.

[42] R. Kumar, N.C. Acikbas, B. Basu, F. Kara, H. Mandal, Microstructure–mechanical properties–wear resistance relationship of SiAlON ceramics, Metallurgical and Materials Transaction A 40A (2009) 2319–2332.

[43] A.G. Evans, E.A. Charles, Fracture toughness determinations by indentation, Journal of the American Ceramic Society 59 (1976) 371–372.

[44] H. Mohrbacher, J.P. Celis, J.R. Roos, Laboratory testing of displacement and load induced fretting, Tribology International 28 (5) (1995) 269–278.

[45] P.Q. Campbell, J.P. Celis, J.R. Roos, O. VanDer Biest, Fretting wear of selected ceramics and cermets, Wear 174 (1–2) (1994) 47–56.
[46] T. Mosmann, Rapid colorimetric assay for cellular growth and survival: application to proliferation and cytotoxicity assays, Journal of Immunological Methods 65 (1–2) (1983) 55–63.
[47] P. Greil, G. Petzow, H. Tanaka, Sintering and HIPing of silicon nitride–silicon carbide composite materials, Ceramics International 13 (1) (1987) 19–25.
[48] A. Bellosi, G. De Portu, Hot-pressed Si_3N_4–SiC whisker composites, Materials Science Engineering A 109 (1989) 357.
[49] J.F. Yang, T. Ohji, T. Sekino, C.L. Li, K. Niihara, Phase transformation, microstructure and mechanical properties of Si_3N_4/SiC composite, Journal of the European Ceramic Society 21 (12) (2001) 2179–2183.
[50] B. Albert, A. Johanson, J. Lewis, M. Raff, K. Roberts, P. Walter, Molecular Biology of the Cell, 4th ed., God and Science, 2002.